Thermal Conductivity and Compression Measurements of a Composite GDL-MPL Material

R. Bock[a,b], A. Shum[d], T. Khoza[c], F. Seland[b], N. Hussain[c], I. Zenyuk[d], O.S. Burheim[a]*

[a] Department of Electrical Engineering and Renewable Energy, Norwegian University of Science and Technology, 7491 Trondheim, Norway.
[b] Department of Materials Science and Engineering, Norwegian University of Science and Technology, 7491 Trondheim, Norway.
[c] Department of Chemical Engineering, University of Cape Town, Rondebosch 7701, South Africa
[d] Department of Mechanical Engineering, Tufts University, MA 02155, USA

*Corresponding Author: Odne.S.Burheim@ntnu.no

MPL and GDL in a PEM fuel cell assembly are often treated as separate layers in the literature. However, there exists a considerable interfacial region where the two different materials merge. The MPL consists of fine carbon particles, a binder and a solvent that is applied on top of the fibrous GDL. In the process of coating, the MPL intrudes into the GDL and forms an MPL-GDL-composite region. This region has properties that differ from either of the materials that it consists of.
Through-plane thermal conductivity and thickness variation under different compaction pressures were measured for such a composite region of commercial gas diffusion layer (GDL), Freudenberg H1410, and custom-made MPL. Thermal conductivity at 9.2 bar compaction pressure for GDL only is 0.111 ± 0.009 W K^{-1} m^{-1}, for MPL only 0.08 ± 0.02 W K^{-1} m^{-1}, and for the composite region is 0.124 ± 0.005 W K^{-1} m^{-1}. X-Ray Computed Tomography images of the materials ascertain the level of penetration for the MPL into the GDL.

Introduction

Hydrogen can be processed from almost any energy source and is the fuel with the highest available gravimetric energy density. An efficient and dynamic technology to convert the free energy of the hydrogen-oxygen chemical reactions is the Polymer Electrolyte Membrane Fuel Cell (PEMFC). When considering automotive applications for instance, thermal management, degradation, and cost reductions are important factors for commercial deployment and success.

A PEMFC consists of several components, i.e. the membrane electrode assembly (MEA) which consists of a membrane (PEM) coated with catalyst layers (CL) on each side that is sandwiched between a thin MPL and a somewhat thicker GDL on each side.

All of these regions have different properties and in some regions, like for the GDL, a great variety of materials with very different properties is available. Over the latest decade,

several efforts have led to more knowledge about the thermal conductivity of these materials. An outline of the development follows.

1. Vie and Kjelstrup were among the first to report thermal conductivities for PEMFC components (1).
2. Khandelwal and Mench reported thermal conductivity for Toray carbon paper TGP-H-60 and TGP-H-90 as well as dry Nafion in different papers (2).
3. Ramousse et al. reported thermal conductivity for GDLs (Quintech and SGL) and the contact to the apparatus (3).
4. Burheim et al. later found a way to separate the contact resistance between the measurement apparatus. (4, 5) They were able to study and differentiate between apparatus sample and sample-sample thermal resistance. They also showed how water changes the thermal conductivity of several materials, e.g. Toray, Sigracet-SGL, Freudenberg, Solvicore, ETEK-ELAT, and Nafion.
5. The next important knowledge development was in-plane thermal conductivity (6-8). Depending on compaction pressure, the difference between in-plane and through-plane thermal conductivity was readily proposed and interpreted in thermal models because it is similar for the electric thermal conductivity (9).
6. Next, the thermal conductivity of the MPL was investigated (10-12) and later (13) and (14).
7. The last PEMFC region's thermal conductivity to be investigated is the catalyst layer's (15).

Generally, these studies together suggested and agreed that at room temperature for dry materials, the through-plane thermal conductivity of an ELAT GDL is around 0.2 $W K^{-1} m^{-1}$, a Sigracet GDL 0.3-0.4 $W K^{-1} m^{-1}$ and Toray GDL is 0.3-0.8 $W K^{-1} m^{-1}$. Changes in temperature lead to changes in thermal conductivity for GDLs. These were measured both for in- and through-plane thermal conductivity by Zamel et al. (8). It is the knowledge from points 1. and 2. that were available to Bapat and Thynell (16) and Kandlikar and Li (17) for their reviews of heat conduction effects in PEM fuel cells in 2007 and thermal management in PEM fuel cell stacks in 2009, respectively.

PTFE is found to decrease the through-plane thermal conductivity of every type of GDL. This is a common conclusion among all studies that includes varying the PTFE content. The common understanding in the literature appears to be that under the absence of PTFE and when a GDL is compressed, more fiber-to-fiber contacts are produced leading to an increase of the effective thermal conductivity. In the presence of PTFE the uncompressed thermal conductivity of a GDL is increased by PTFE conducting some heat between the carbon fibers (18). As soon as the GDL is compressed, the PTFE only inhibits more fiber to fiber contacts and then the effective through-plane thermal conductivity of the GDL is lowered in the presence of PTFE. This is observed even as the smallest portion of PTFE is added to the GDL.

The thermal conductivity of different MPL made for PEMFC were, to our knowledge, for the first time investigated independently of any other fuel cell components (13). The value was found to vary between 0.06 and 0.10 $W K^{-1} m^{-1}$ at compaction pressures from 5 to 16 bar. Despite being among the thinnest layers of a PEMFC, the MPL has a thermal conductivity so low that it still has a significant effect on the overall temperature distribution in a PEMFC. A recent study by Thomas et al. showed that the temperature gradient across this layer contribute to water transport and that this increase in temperature helps keeping the water in the MPL in a gas phase (11).

MPL and GDL are often treated as separate layers in the literature. There exists, however, an interfacial region where the two layers merge into one another and thus form a third layer. The fine material of the MPL can intrude considerably into the fiber structure of the GDL material. This composite region has physical properties that are unlike those of both of the original layer materials (14).

When developing these properties, both experiments and modelling are required. For instance, it is experimentally demonstrated that there is a strong correlation between local degradation and local temperature profiles (19), although PEMFCs are shown to last for 26000 hours or three years continuous operation (20). In order to investigate this and similar effects further, detailed knowledge about local heat production, local thermal conductivity, thermo-mechanical stress, etc. is required. Kandlikar and Li summarize this very well in 2009 (17) by discussing literature available at the time and presenting a thermal model. Bapat and Thynell gave a separate review on thermal PEMFC modelling already in 2007 (16). Since then several developments of the available knowledge of PEMFC thermal conductivity have emerged. Zamel and Li gave an overview on PEMFC mechanical properties (21), also including thermal conductivity, but even over the last three years the knowledge and understanding of PEMFC material's thermal conductivity have progressed further, especially with respect to understanding the MPL-GDL-composite interface region and its properties.

The temperature difference across the PEMFC can reach several °C despite being less than a millimeter thick between the bipolar gas flow plates. Temperature differences arise mainly across the GDL, as heat is generated where the chemical reaction takes place, in the catalyst layers close to the membrane, especially on the cathode side, as demonstrated by Pharaoh et al. (9). Several research efforts have led to a good understanding of the thermal conductivity of the GDL and how it changes with compaction pressure, temperature, PTFE content, varied fabrics, and water content (4, 5).

The most thorough review available on this topic is, to the authors' knowledge, one by Zamel and Li (21). For the PTL, the in-plane and through-plane thermal conductivities are different. Because the in-plane electrical conductivity is several times larger than the through-plane electrical conductivity, it was first postulated (22, 23) and later verified experimentally (6, 8) that the in-plane thermal conductivities are five to ten times larger than the through-plane ones (mainly depending on the GDL compaction).

In this work, we introduce a way of producing samples that consist purely of merged MPL-GDL material. We then measure the thermal conductivity and compressibility as compared to an untreated sample of the same GDL. These values are compared to available literature.

Experimental

Production of MPL-GDL-composite material

A doctor blade setup was selected to drench a commercially available GDL, Freudenberg H1410, with a custom-made MPL ink slurry.

An ink slurry was produced containing 11.9 wt% solid materials, a recipe formerly used and chosen here for reference (14). Vulcan EC-XC72R-50 was weighed and transferred into a bead mixing bowl. Subsequently, a known amount of surfactant (Triton X114), was mixed with a known amount of water before mixing with the carbon powder and PTFE solution. The bowl was then placed into the bead mixing device and rotated at 400 rpm for

30 minutes. Then, the ink was separated from the beads and weighed. The correct amount of 60% PTFE solution to achieve 20wt% relative to carbon weight was calculated, weighed and added to the ink slurry. It was carefully mixed again with a grinder. The ingredients and their amounts can be reviewed in Table I.

TABLE I. Ink slurry recipe (11.9 solids wt%, 20 wt% PTFE relative to carbon weight)(24). Actual masses used in producing the applied ink slurry shown.

Component	Mass (g)	Comments
Carbon, Vulcan EC-XC72R-50	2.008	powder
Triton X-114	3.994	surfactant
Water, deionized	13.56	18MΩ@25°C
PTFE solution (60wt% PTFE)	0.622	= 0.373g pure PTFE
Total	20.184	

The GDL substrates that were to be coated were placed on the glass plate of a doctor blade setup and fixed in position. The doctor blade was filled with ink and adjusted to make a single coating of 25 μm thickness at a speed of 2.5 mm s^{-1}. To remove the resulting 25 μm thick MPL on top, a second doctor blade was placed right behind the first when coating, so that it would scrape off the MPL on top, leaving only MPL soaked GDL material. These samples are referred to as "wet scraped" later on. The GDL was then dried at 100 °C for 5 minutes and then the coating procedure was repeated for the remaining uncoated side. Afterwards, the coated GDL was dried at 100 °C for one hour before it was baked in an oven at 350 °C for one hour.

SEM imaging

SEM images of a cross section of the composite material were taken with a FEI NOVA NANOSEM 230 to confirm visually that the GDL material is infused with the MPL material throughout its thickness. The samples were submerged in liquid nitrogen for one minute and then cut across with a cooled scalpel. The SEM images were taken at 20 keV and have a magnification factor of 1000.

X-Ray Computed Tomography

The X-ray computed tomography (CT) experiments were conducted at Beamline 8.3.2. at the Advanced Light Source (ALS) at Lawrence Berkeley National Laboratory, CA, USA. The source energy was 14 keV and the optics system consisted of a sCMOS PCO.Edge camera, 0.5 mm LuAG scintillator and 5x lenses, resulting in a pixel resolution of 1.33 μm. Additional details of the experimental set-up are provided by Zenyuk et al. in (25), where fine-thread stamp was used to image GDLs under three levels of compression. The working field of view (FOV) for image processing was cropped to 2.2 x 2.2 mm. Image processing was done with ImageJ (Fiji).

Thermal conductivity and compression measurements

A custom-made measuring rig was designed and constructed to simultaneously measure the variables that appear in the discrete form of Fourier's law, the heat flux q, the temperature drop over the sample T_{45} and the sample thickness δ_{45} while applying a compaction pressure with a pneumatic actuator, see Fig. 4 (15). Thus, values for thermal

conductivity k and for the compression of the materials under different compaction pressures were obtained.

The sample is made up of circular samples with a diameter of 21 mm that were punched out of a sheet of the pure GDL material and the composite material each. To establish a steady heat flux the temperature on the hot side was held at 35 °C while the temperature on the cold side was maintained at 10 °C such that the sample temperature is very close to room temperature of 22 – 23 °C.

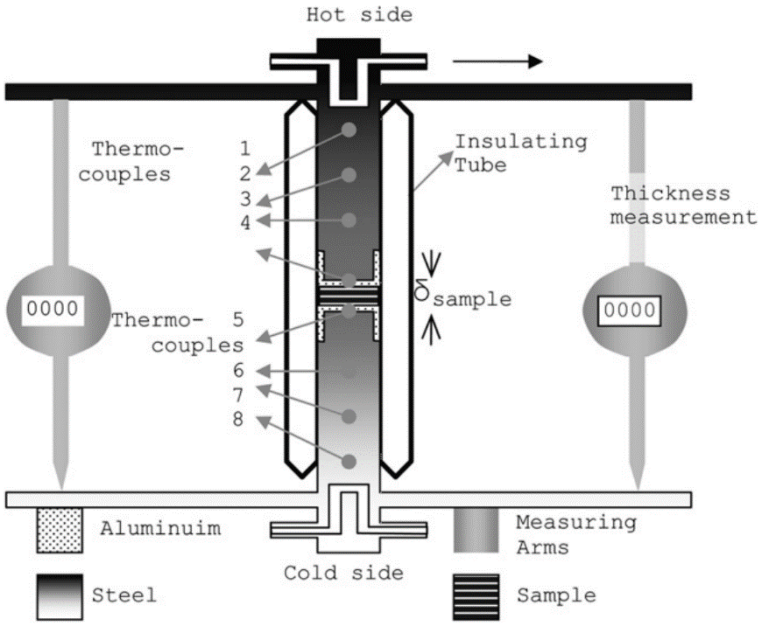

Figure 4. 2D sketch of the apparatus used to measure thermal conductivity and compaction as reported here (15)

The samples were given 10 minutes to reach steady state in terms of heat flux through them as well as compaction state. The heat flux was then recorded at 30-second intervals for 10 minutes and averaged. To investigate the thermal conductivity the heat flux q_{sample} was measured for one sample first, then for three samples on top of each other and finally for five samples on top of each other. The sample sample thermal contact resistance is negligible, according to Burheim et al. (10). The samples were subsequently measured a compaction pressure of 2.3 bar, 4.6 bar, 6.8 bar and 9.3 bar. The thickness of the sample stack was recorded and a thermal resistance R_{total} was obtained for every sample stack, see Eq. [1].

$$R_{\text{total}} = \frac{(T_4 - T_5)}{q_{\text{sample}}} \quad [1]$$

with

$$q_{\text{sample}} = \frac{(q_{\text{upper}} + q_{\text{lower}})}{2} \quad [2]$$

$$q_{\text{upper}} = \mathrm{k}_{\text{steel}} \frac{(T_1 - T_3)}{\delta_{13}} \quad [3]$$

$$q_{\text{lower}} = \mathrm{k}_{\text{steel}} \frac{(T_6 - T_8)}{\delta_{68}} \quad [4]$$

The heat flux through the sample q_{sample} is obtained by averaging the heat fluxes of the upper and lower steel cylinder, q_{upper} and $q_{lower,}$ Eq. [2]. These heat fluxes are obtained by measuring temperature differences over known distances δ_{xx} between thermocouples and multiplying with the thermal conductivity of the steel k_{steel}, Eqs. [3] and [4].

The thermal conductivity apparatus was calibrated using materials with known thermal conductivity, thus obtaining a value for $k_{steel,}$ see Ref. (5). These values are known with 5% accuracy and thus this is the accuracy limitation of the reported values in this manuscript.

Results and discussion

SEM imaging

Fig. 1, left side shows a cross section of an untreated piece of Freudenberg H1410 GDL material. This material has not been treated with PTFE by the manufacturer All that is visible are the fibers and hints of binder material. Fig. 1, right side shows a cross section of the same GDL material after the custom-made MPL ink slurry was applied, wet scraped, dried and the sample was sintered. It suggests that the MPL ink slurry has fully penetrated the GDL material. There is no MPL layer to be seen on top of the GDL, as it has successfully been removed by the rotated doctor blade setup. Hence, the creation of a pure composite material was successful.

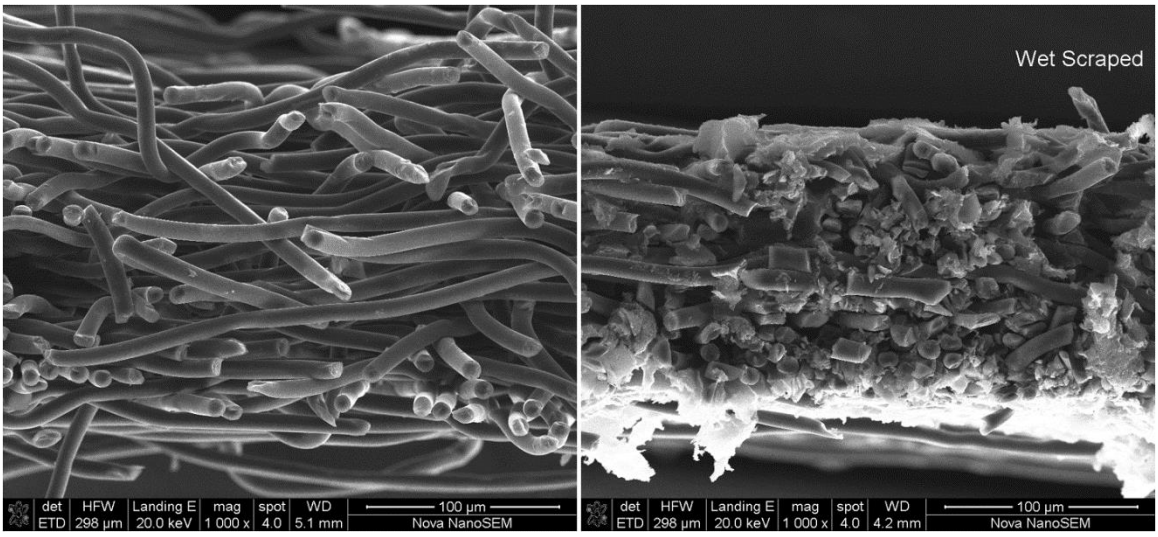

Figure 1. Left: Cross-section SEM image of pure Freudenberg H1410 GDL material before application of the MPL ink slurry. Right: Cross-section SEM image of GDL/MPL composite material after manual application of the MPL ink slurry and scraping off residual MPL from on top of the material.

X-Ray Computed Tomography

The image in Fig. 3 shows two different cross-sections. a) shows a sample of Freudenberg H1410 that has been coated with the custom-made MPL and the MPL on top was removed directly after. b) shows a sample of Freudenberg H1410 that has been coated with the custom-made MPL, but the MPL on top was not removed for comparison. In addition to these cross-sections, c) shows an in-plane view of the wet-scraped composite material. A nice contrast between fiber and MPL material was achieved through image analysis.

These X-Ray CT images indicate that the MPL ink slurry has completely soaked the GDL substrate material. The in-plane view clearly shows that MPL material has settled in-between the GDL fibers. These CT images support the claim of having produced pure composite material.

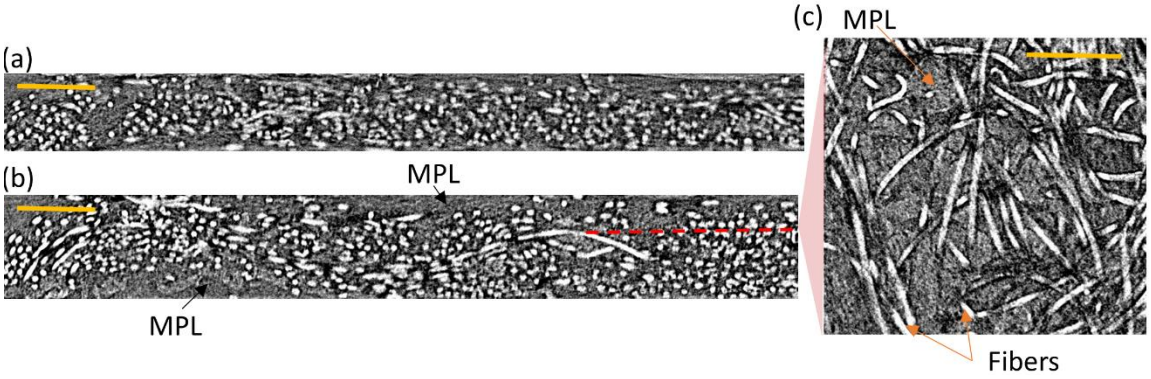

Figure 3. X-Ray CT image of the composite material showing cross sections in a) of a sample where the MPL-on-top was removed and b) a sample with intact MPL-on-top, as well as an in-plane view of GDL fibers and MPL in c). The scale bar is 150 μm.

Thermal conductivity

The thermal resistance of the sample and its contact to the apparatus were plotted as a function of the measured thickness in order to de-convolute the thermal conductivity and the thermal contact resistance.

$$R_{\text{tot}} = 2R_{\text{contact}} + \frac{\delta_{\text{sample}}}{k_{\text{sample}}} \quad [5]$$

The inverse of the gradient of thermal resistance with thickness is the thermal conductivity, see Eq. [5] (10). Thus, the slope of a linear regression of the obtained thermal resistance results is the average thermal conductivity of all sample stacks.

At a compaction pressure of 9.2 bar the thermal conductivity of untreated Freudenberg H1410 (114 μm), was found to be 0.111±0.009 W K^{-1} m^{-1} and for the custom-MPL-coated Freudenberg H1410 material it was 0.124±0.005 W K^{-1} m^{-1}. The untreated Freudenberg H1410 material was compacted to 87% of its original thickness at 9.2 bar compaction pressure. The MPL-treated H1410 material was compacted to 77% of its original thickness at 9.2 bar compaction pressure, see Table II for results at different compaction pressures.

TABLE II. Thermal conductivity k and compression measurement results.

Compaction pressure [bar]	**Freudenberg H1410 untreated**		**Freudenberg H1410 composite**	
	k [W / m K]	compaction	k [W / m K]	compaction
2.3	0.104 ± 0.016	96 %	0.108 ± 0.003	82 %
4.6	0.106 ± 0.011	91 %	0.115 ± 0.004	79 %
6.9	0.109 ± 0.013	89 %	0.120 ± 0.003	78 %
9.2	0.111 ± 0.009	87 %	0.124 ± 0.005	77 %

The MPL-treated Freudenberg H1410 has a larger compression from atmospheric pressure to first compaction pressure, but a less steep compression gradient with rising compaction pressure than the original H1410 material, see Fig. 5.

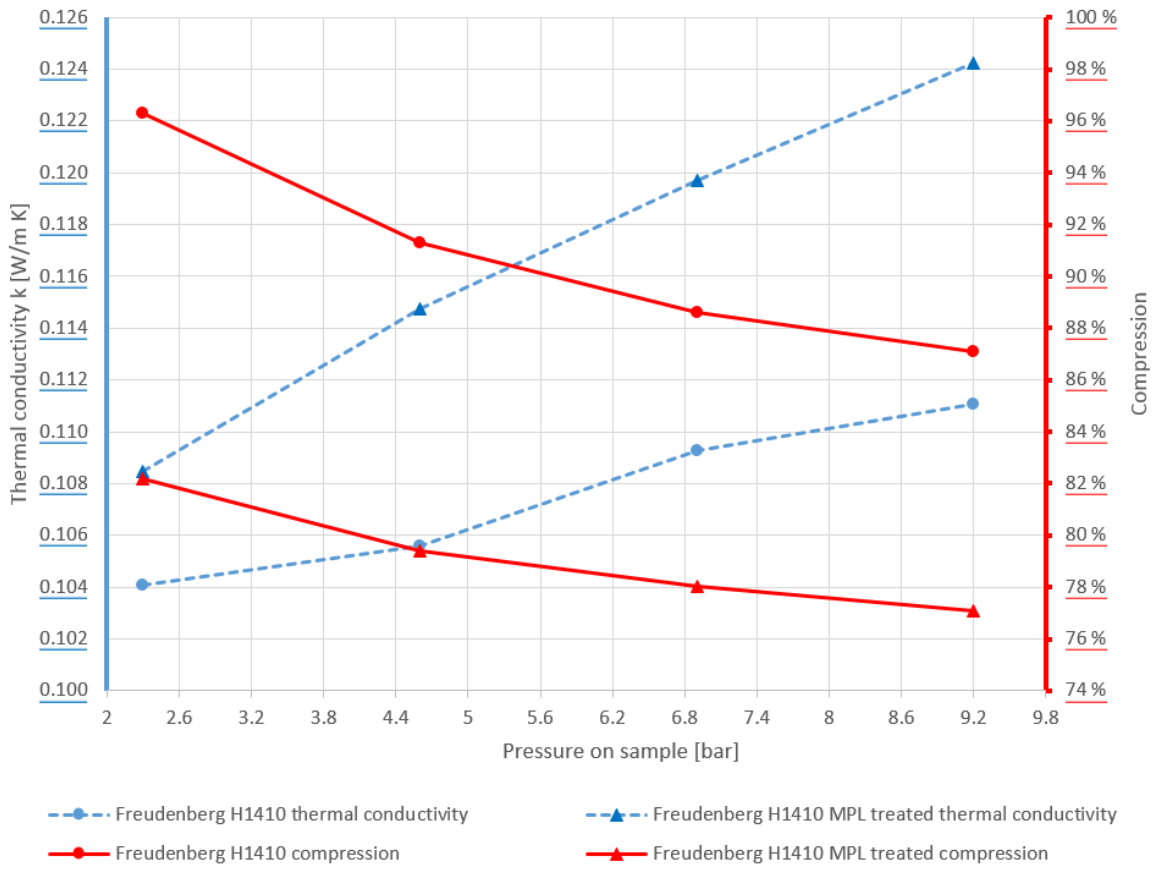

Figure 5. Plot of thermal conductivity k and compaction for untreated Freudenberg H1410 and the custom-made composite material based on Freudenberg H1410

Thermal conductivity for the composite material is found to be higher than that of the pure GDL material. This is the case even though MPL material alone has a low thermal conductivity, 0.08 ± 0.02 W K^{-1} m^{-1} in the case of a very similar MPL as reported in (14). The fact that a material consisting of two materials with low thermal conductivity (GDL-only and MPL-only) comprise a material with a higher thermal conductivity (the composite) might appear contradictory but must be seen in the light of similar materials as pointed out in a previous work from our group (14). There, graphitized carbon fibers are mentioned that make up polymer composite heat exchangers. The fiber's thermal conductivity is low individually but was reported to be several times larger than that individual value when bundled into a composite (26).

In the case of our composite we have a region that consists of two materials with low thermal conductivity, but that together comprise a material with higher thermal conductivity. It seems that even though the MPL material has a lower thermal conductivity when compared to the GDL fibers, it still manages to enhance the heat transfer from fiber to fiber by increasing the contact surface between two fibers.

The drenching of the GDL with MPL ink slurry and the subsequent sintering seem to have weakened the mechanical strength of the GDL material. The composite is compacted to 77 % of original thickness at a compaction pressure of 9.2 bar as opposed to 87 % of original thickness for the untreated GDL at the same compaction pressure. The binder that is applied to the GDL fibers by the manufacturer seems to be washed and/or burnt away during the preparation process chosen for the composite material. This should then also lower the thermal conductivity, as the binder enhances thermal contact between GDL fibers

greatly. The fact that the thermal conductivity is increased by treating the GDL with MPL ink slurry nonetheless supports the theory that the contact surface area between fibers is greatly enlarged by the MPL, thus increasing thermal transport even though the MPL material has low thermal conductivity itself.

The thermal conductivity at 9.2 bar compaction pressure of another untreated Freudenberg GDL, namely H2315 (182 μm), was reported by us earlier (4) to be 0.15±0.02 W K^{-1} m^{-1}, roughly 50% higher than for the H1410 we measured. This complies with a trend seen in Toray paper, where the thermal conductivity at 9.3 bar compaction increases with thickness from 0.53±0.03 W K^{-1} m^{-1} for Toray TGP-H-060 (165 μm) to 0.65±0.02 W K^{-1} m^{-1} for Toray TGP-H-090 (265 μm) and to 0.81±0.03 W K^{-1} m^{-1} for Toray TGP-H-120 (333 μm). (4)

Conclusion

The way the GDL is produced, the Teflon content, and the binder content all have influence on the final value of the thermal conductivity for a GDL material. Toray paper has a higher thermal conductivity when the thickness increases. An increase in PTFE content will lower the thermal conductivity. In general, Freudenberg GDLs have a far lower thermal conductivity than other commercially available GDLs.

By depositing MPL material into the GDL, thermal contact between GDL fibers is enhanced, hence the overall thermal conductivity of the material increases. This could be a way to improve thermal conductivity of GDL materials with low thermal conductivity to achieve improved temperature management in PEM fuel cells.

Acknowledgments

Financial support from the Norwegian University of Science and Technology through the Strategic Research Program ENERSENSE is greatly acknowledged.

The Advanced Light Source is supported by the Director, Office of Science, Office of Basic Energy Sciences, of the U.S. Department of Energy under Contract No. DE-AC02-05CH11231. The authors would like to acknowledge the assistance of Dula Parkinson with the experimental set-up at the beamline.

References

1. P. J. S. Vie and S. Kjelstrup, *Electrochimica Acta*, **49**, 1069 (2004).
2. M. Khandelwal and M. M. Mench, *Journal of Power Sources*, **161**, 1106 (2006).
3. J. Ramousse, S. Didierjean, O. Lottin and D. Maillet, *International Journal of Thermal Sciences*, **47**, 1 (2008).
4. O. S. Burheim, J. G. Pharoah, H. Lampert, P. J. S. Vie and S. Kjelstrup, *Journal of Fuel Cell Science and Technology*, **8**, 021013 (2010).
5. O. Burheim, P. J. S. Vie, J. G. Pharoah and S. Kjelstrup, *Journal of Power Sources*, **195**, 249 (2010).
6. E. Sadeghi, N. Djilali and M. Bahrami, *Journal of Power Sources*, **196**, 3565 (2011).
7. P. Teertstra, G. Karimi and X. Li, *Electrochimica Acta*, **56**, 1670 (2011).

8. N. Zamel, E. Litovsky, X. Li and J. Kleiman, *international journal of hydrogen energy*, **36**, 12618 (2011).
9. J. G. Pharoah and O. S. Burheim, *Journal of Power Sources*, **195**, 5235 (2010).
10. O. S. Burheim, G. Ellila, J. D. Fairweather, A. Labouriau, S. Kjelstrup and J. G. Pharoah, *Journal of Power Sources*, **221**, 356 (2013).
11. A. Thomas, G. Maranzana, S. Didierjean, J. Dillet and O. Lottin, *International Journal of Hydrogen Energy*, **39**, 2649 (2014).
12. M. Andisheh-Tadbir, E. Kjeang and M. Bahrami, *Journal of Power Sources*, **296**, 344 (2015).
13. O. S. Burheim, H. Su, S. Pasupathi, J. G. Pharoah and B. G. Pollet, *International Journal of Hydrogen Energy*, **38**, 8437 (2013).
14. O. S. Burheim, G. A. Crymble, R. Bock, N. Hussain, S. Pasupathi, A. du Plessis, S. le Roux, F. Seland, H. Su and B. G. Pollet, *International Journal of Hydrogen Energy*, **40**, 16775 (2015).
15. O. S. Burheim, H. Su, H. H. Hauge, S. Pasupathi and B. G. Pollet, *International Journal of Hydrogen Energy*, **39**, 9397 (2014).
16. C. J. Bapat and S. T. Thynell, *Journal of Heat Transfer*, **129**, 1109 (2007).
17. S. G. Kandlikar and Z. Lu, *Journal of Fuel Cell Science and Technology*, **6**, 044001 (2009).
18. J. Yablecki, A. Nabovati and A. Bazylak, *Journal of The Electrochemical Society*, **159**, B647 (2012).
19. F. Nandjou, J.-P. Poirot-Crouvezier, M. Chandesris, J.-F. Blachot, C. Bonnaud and Y. Bultel, *Meeting Abstracts*, **MA2015-01**, 1661 (2015).
20. S. J. C. Cleghorn, D. K. Mayfield, D. A. Moore, J. C. Moore, G. Rusch, T. W. Sherman, N. T. Sisofo and U. Beuscher, *Journal of Power Sources*, **158**, 446 (2006).
21. N. Zamel and X. Li, *Progress in energy and combustion science*, **39**, 111 (2013).
22. J. G. Pharoah, K. Karan and W. Sun, *Journal of Power Sources*, **161**, 214 (2006).
23. E. Sadeghi, M. Bahrami and N. Djilali, *Journal of Power Sources*, **179**, 200 (2008).
24. G. A. Crymble, (2014).
25. I. V. Zenyuk, D. Y. Parkinson, G. Hwang and A. Z. Weber, *Electrochemistry Communications*, **53**, 24 (2015).
26. F. Robinson, J. G. Cevallos, A. Bar-Cohen and H. Bruck, in *ASME 2011 International Mechanical Engineering Congress and Exposition*, p. 597 (2011).